# Synaptic Learning and Memory Functions Achieved Using Oxygen Ion Migration/Diffusion in an Amorphous InGaZnO Memristor

*Zhong Qiang Wang, Hai Yang Xu,* Xing Hua Li, Hao Yu, Yi Chun Liu,* and Xiao Juan Zhu*

**A single synaptic device with inherent learning and memory functions is demonstrated based on an amorphous InGaZnO (α-IGZO) memristor; several essential synaptic functions are simultaneously achieved in such a single device, including nonlinear transmission characteristics, spike-rate-dependent and spike-timing-dependent plasticity, long-term/short-term plasticity (LSP and STP) and "learning-experience" behavior. These characteristics bear striking resemblances to certain learning and memory functions of biological systems. Especially, a "learning-experience" function is obtained for the first time, which is thought to be related to the metastable local structures in α-IGZO. These functions are interrelated: frequent stimulation can cause an enhancement of LTP, both spike-rate-dependent and spike-timing-dependent plasticity is the same on this point; and, the STP-to-LTP transition can occur through repeated "stimulation" training. The physical mechanism of device operation, which does not strictly follow the memristor model, is attributed to oxygen ion migration/diffusion. A correlation between short-term memory and ion diffusion is established by studying the temperature dependence of the relaxation processes of STP and ion diffusion. The realization of important synaptic functions and the establishment of a dynamic model would promote more accurate modeling of the synapse for artificial neural network.**

## 1. Introduction

The synapse is the cellular unit for learning and memory,[1,2] and synapse emulation is viewed as a key step toward neuromorphic computing. Some synaptic devices have been developed based on common electronic components.[3–5] However, many transistors and capacitors are used therein to emulate a single synapse, which increases the energy dissipation and limits the density of integration. Moreover, in these artificial neural devices, synaptic behaviors are imitated through software programming. Thus, it is highly desirable to realize synapse emulation in a single device with inherent learning and memory abilities. Recently, the memristor has been proposed to emulate the synapse because of their similar transmission characteristics.[6] Based on ion migration or atomic switch mechanisms, several groups have succeeded in designing and fabricating memristors using different materials (e.g., $TiO_2$, $Ag_2S$, $RbAg_4I_5$, Si:Ag, and $WO_x$);[7–13] some groups have used their memristors to emulate the spike-timing-dependent plasticity (STDP) and transmission characteristics of the synapse. However, a complete analog to the biological synapse is difficult to achieve because not all synaptic functions are involved in the memristor model. Besides ion migration, concentration gradient-induced ion diffusion can bring a new dynamic process to the memristor, thus leading to the appearance of some other synaptic phenomena, such as long-term/short-term memory.[10,13] As for the selection of memristive materials, compared to commonly used polycrystalline films, the amorphous InGaZnO (α-IGZO) film offers certain advantages, including high uniformity over a large area, room-temperature growth conditions, easily controlled electrical properties, and excellent flexibility.[14] The high uniformity and the lack of grain boundaries enable device scaling to nanometer dimensions, thereby facilitating high-density integration. The α-IGZO can be continuously changed from insulator to conductor by adjusting the oxygen content,[15] which makes it suitable for a dynamic response to input signals, as occurs in the biological synapse. Moreover, the flexibility of the amorphous film allows memristors to be bent into irregular shapes in practical applications.

Here, we demonstrate a single synaptic device based on an α-IGZO memristor; several learning/memory functions, similar to the biological systems, are achieved in such a single device. Especially, a "learning-experience" function is obtained for the first time. The physical mechanism of device operation is attributed to oxygen ion migration/diffusion, and a correlation

Dr. Z. Q. Wang, Prof. H. Y. Xu, Dr. X. H. Li, Dr. H. Yu, Prof. Y. C. Liu
Center for Advanced Optoelectronic Functional Materials Research and Key Laboratory for UV-Emitting Materials and Technology of Ministry of Education
Northeast Normal University
Changchun 130024, P. R. China
E-mail: hyxu@nenu.edu.cn; ycliu@nenu.edu.cn
Prof. X. J. Zhu
The institute of Genetics and Cytology
Northeast Normal University
Changchun 130024, P. R. China

**DOI: 10.1002/adfm.201103148**

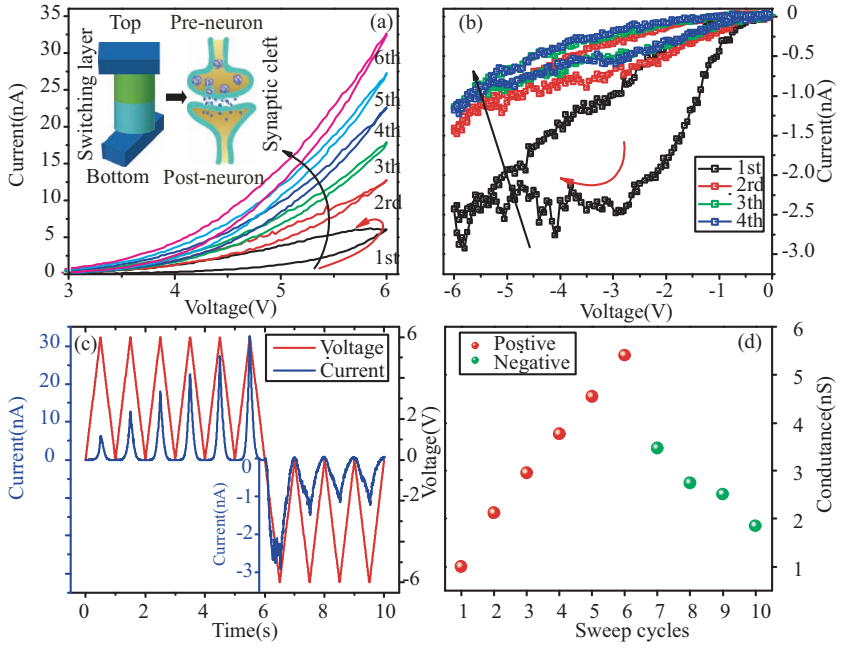


**Figure 1.** The nonlinear transmission characteristics of α-IGZO memristor. a,b) *I–V* characteristics of the memristor at positive and negative bias voltages, the voltage sweep range is from zero to 6 (–6) V then back to zero, and the time for a sweep cycle is 1 s. The device conductivity continuously increases (decreases) during the positive (negative) voltage sweeps. The insets show a structural diagram of the two-terminal, bilayer α-IGZO memristor and a schematic illustration of the concept of using memristors as synapses between neurons. c) The curves of current and voltage versus time, which are plotted from the data in a and b. d) The variation of the device conductivity with the scanning cycles.

between short-term memory and ion diffusion is established by investigating their relaxation process at different temperatures. The present work would promote a more accurately model of the synapse for use in artificial neural networks.

## 2. Nonlinear Transmission Characteristics

A synapse can be regarded as a two-terminal device and the synaptic weight can be dynamically modified and stored using consecutive spikes,[1,16] which is similar to a charge-controlled memristor.[6] Inspired by the memristor model, the switching layer of our synaptic device consists of two parts: the conducting (oxygen-deficient) and insulating (oxygen-rich) α-IGZO layers (inset of **Figure 1**a). As shown in Figures 1a and b, when consecutive positive (0 to 6 V) and negative (0 to –6 V) voltage sweeps are applied to the device, its conductivity continuously increases and decreases, respectively, with the voltage sweep. To clearly illustrate such a changing trend, the curves of current and voltage versus time, as well as the conductivity measured at the end of each sweep, are plotted in Figure 1c,d. The device conductivity can also be adjusted by tuning the duration and amplitude of the applied voltage pulses. Higher-amplitude and longer-duration pulses cause a larger change in the conductivity, as illustrated in **Figure 2**a. If we treat the device conductivity as a synaptic weight, the above phenomena show a close similarity to the nonlinear transmission characteristic of biological synapses. Positive/negative pulses are used to excite/inhibit the synapse. The modulation of conductance can be considered as a result of the motion of the conduction front between oxygen-rich and oxygen-deficient layers, which is realized by the electric field induced migration of oxygen ions. Note that there are also some behaviors that can not be explained by the memristor model. Figure 2b shows the current response to a series of 100 positive voltage pulses (5 V, 100 ms, "P process") immediately followed by 80 negative pulses (–5 V, 100 ms, "N process"). Although the conductivity also increases (decreases) under the stimulation of consecutive positive (negative) pulses, a gap is observed between the final state of the "P process" and the initial state of the "N process". These two states should have been the same in the frame of the memristor model. Such a phenomenon, along with some following observations different from the memristor, can be understood by considering the back-diffusion effect of oxygen ions and will be discussed below.

## 3. Synaptic Plasticity: Spike-Rate-Dependent Plasticity and Spike-Timing-Dependent Plasticity (STDP)

An important characteristic of the synapse is its plasticity. One aspect of synaptic plasticity is the temporal correlation between different spike signals. Firstly, the synaptic weight can be

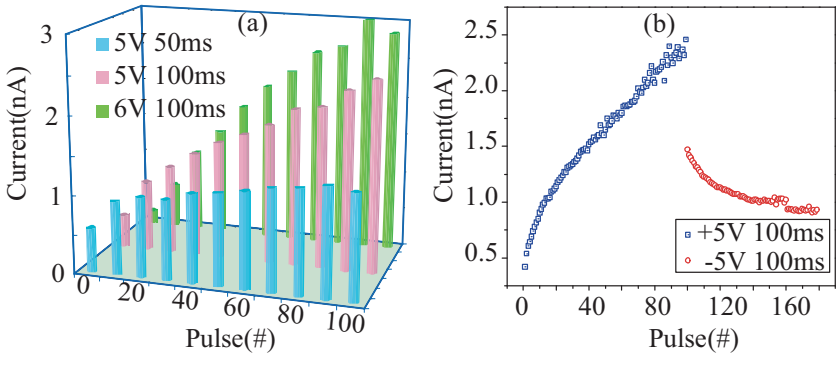


**Figure 2.** Memristor response to programming pulses. a) Higher-amplitude and longer-duration pulses cause a larger change in the device conductivity; and, b) The device conductivity can be increased or decreased by consecutive potentiating or depressing pulses. All the current data in (a) and (b) are recorded using a read voltage pulse with amplitude 3 V and duration 50 ms.

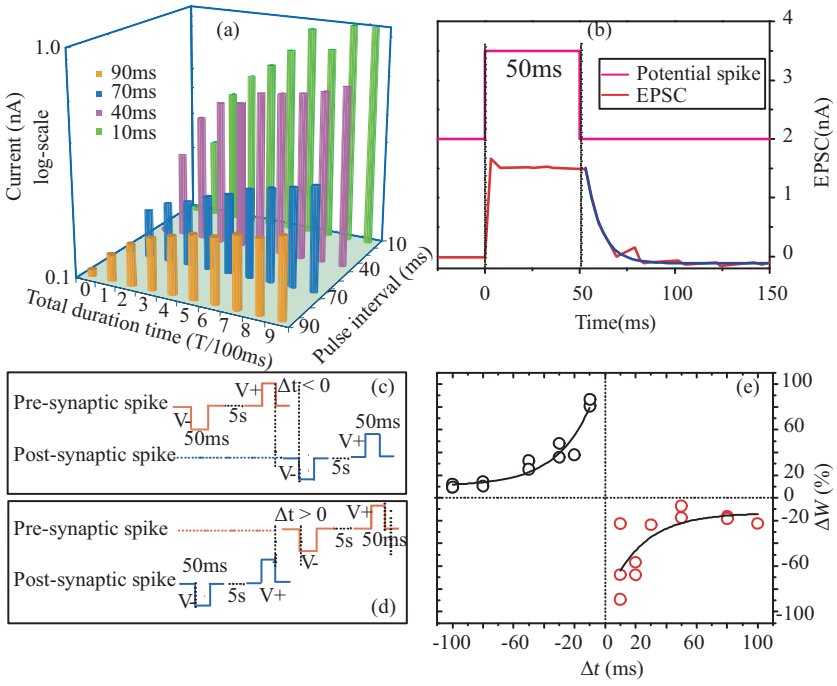


**Figure 3.** Demonstration of spike-rate-dependent plasticity and STDP in the memristor synapse. a) The variation of the current (log-scale) with the pulse interval (the pulse duration and number are fixed herein), which indicates that the high stimulation rate can result in the conductance enhancement. b) The formation and decay of spike-induced EPSC. c,d) A pair of the pre- and post-synaptic spikes, which are designed to implement STDP. e) The relative change of the memristor synaptic weight ($\Delta W$) versus the relative spike timing ($\Delta t$). The solid lines are the exponential fits to the experimental data.

modified by temporally correlated pre- and post-synaptic spikes via STDP, which is one of the essential learning/memory laws for emulating synaptic functions.[5,8,11,12] When a post-synaptic spike is triggered momentarily (a few milliseconds) after a pre-synaptic spike, the synaptic weight increases and long-term potentiation occurs; in converse, when the temporal order is reversed, the synaptic weight decreases and long-term depression occurs.[16–19] Secondly, the change of synaptic weight strongly depends on the spike rate (i.e., the time interval between stimuli). On these two points, a remarkable similarity is observed between the current device and the biological synapse.

In the current device, the top and bottom electrodes can be seen as the pre- and post-synaptic neurons, respectively. Considering the charge-controlled memristor model, if we fix the total spiking time, the change of synaptic weight should be constant and be independent of the spike rate. However, for the current device, a different phenomenon that more frequent stimulation leads to a larger change of synaptic weight is observed (**Figure 3**a). Such a spike-rate-dependent characteristic is similar to that of biological synapses,[20] and may be ascribed to the temporal interaction between the excitatory postsynaptic current (EPSC) and the spike. As shown in Figure 3b, a single presynaptic spike (5 V, 50 ms) can trigger an EPSC, with its intensity gradually decaying to zero within around 50 ms after the pulse passes. It is conceivable that after the pulse voltage is removed, the oxygen ions still can move forward a short distance due to the inertia effect, which may result in the formation of ion-mediated EPSC.

In the case of a high spike rate, the EPSC does not disappear completely when the next pulse is reached. Their overlap accelerates ion migration, thus leading to a larger change in the conductivity. Furthermore, the synaptic weight can be modulated by the degree of overlap between EPSC and spike, that is, by the pulse interval. The observed spike-rate-dependent characteristic is similar to the STDP rule of biological synapses. Through the EPSC-spike interaction, the presynaptic neuron can also produce spatial and temporal correlations with postsynaptic neuron.[1] To implement STDP, a pair of pulses with amplitude $V^+/V^- = 5$ V/–5 V are applied to the top and bottom electrodes as the pre- and post-synaptic spikes, as illustrated in Figure 3c,d. In both pre- and post-synaptic spikes, there is 5 s interval between the $V^+$ and $V^-$, which is long enough to ignore the effect of $V^+$ on $V^-$ according to the decay time of EPSC. The relative timing $\Delta t < 0$ ($\Delta t > 0$) is defined as the interval from the end of the presynaptic (postsynaptic) spike to the beginning of the postsynaptic (presynaptic) spike. The postsynaptic currents were measured before ($I_1$) and 15 min after ($I_2$) the spike-pair application. That is, we record the long-term memory level herein (including in the above spike rate response measurements), which will be discussed in the next section. The relative change of synaptic weight ($\Delta W$) is defined as $(I_2 - I_1)/I_1$. Figure 3d shows the variation of $\Delta W$ with $\Delta t$. We can see that i) when the presynaptic neuron spikes before (after) the postsynaptic neuron, the synaptic weight increases (decreases); ii) the smaller the time interval $\Delta t$, the larger the absolute value of $\Delta W$; and, iii) the experimental data can be well fitted to a exponential function. These are typical STDP characteristics of biological synapses.[16–19] In fact, the temporal characteristic is identical between spike-rate-dependent plasticity and STDP behaviors, and frequent stimulation can increase the synaptic weight (namely, the device conductivity, which can also be regarded as the memory level.).

## 4. Synaptic Plasticity: Long-Term/Short-Term Plasticity and "Learning-Experience" Function

Synaptic plasticity can be categorized into long-term and short-term plasticity (LTP and STP) according to the memory retention; in psychology, these correspond to the long-term and short-term memory behaviors, respectively.[21–23] The STP (LTP) is a temporary (permanent) potentiation of neural connections, and lasts for a few minutes or less (from hours to years). Besides, STP can be converted to LTP through repeated rehearsals, which involves a physical change in the structure of neurons. These temporal characteristics of memory retention were also achieved in the current device.

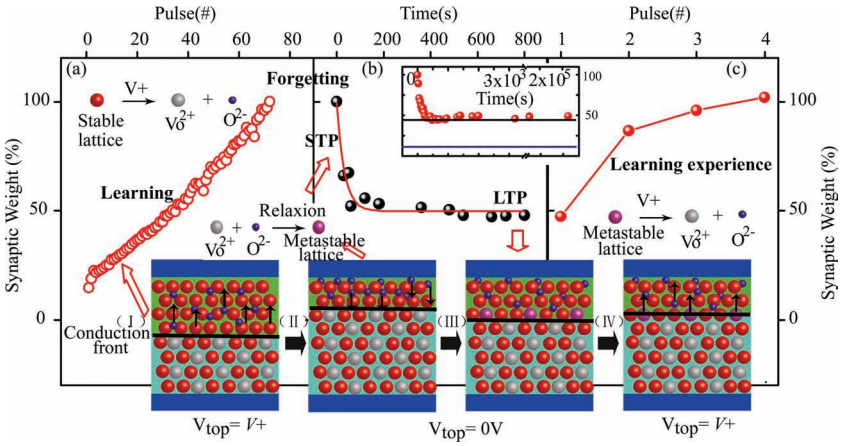


**Figure 4.** The LTP/STP and "learning-experience" behaviors, and the dynamic model of device operation. a) Nearly linear increase of the synaptic weight with consecutive stimuli. b) The spontaneous decay of the conductivity, that is, the relaxation process of STP, which is very similar to the human-memory "forgetting curve". The solid lines are an exponential decay fits to the experimental data using Equation 1. c) Re-stimulation process from the mid-state. Only four pulses, far fewer than the number of stimuli required in the first learning process, can make the device recover its memory, which bears striking resemblance to the learning process based on experience for biological systems. The top inset presents the memory retention of LTP, and the bottom inset illustrates an oxygen ion migration/diffusion model of device operation.

**Figure 4**a shows the results of a test in which the synaptic device was stimulated sequentially with 100 positive pulses; the synaptic weight gradually increases with the number of pulses. It is interesting to note that when the applied voltage is removed, a spontaneous decay of synaptic weight occurs in the case of no external inputs (Figure 4b). The decay rate is very fast at the initial stage and then gradually slows down. Such a changing trend is consistent with the human-memory "forgetting (or retention) curve" in psychology. The synaptic weight does not relax to the initial state, but stabilizes at a mid-state, which means that the change of synaptic weight consists of two parts: STP and LTP. Many researchers have attempted to develop different mathematical models for the quantitative description of memory loss in biological systems.[10,13] However, which mathematical function best portrays memory loss is still a subject of hot debate. Recently, Ohno et al. and Chang et al. used an exponential power function and a stretched-exponential function, respectively, to quantitatively study the STP behavior of their synaptic devices.[10,13] A common feature of the two equations is to contain an exponential decay term. Thus, for simplicity, we use an exponential decay equation to describe the relaxation process of STP

$$M(t) = M_e + (M_0 - M_e)\exp(-t/\tau) \quad (1)$$

$M(t)$, $M_0$, and $M_e$ are the memory level at time $t$, $t = 0$, and at steady state after a long time, and, $\tau$ is the relaxation time constant, which can be used to evaluate the forgetting rate. The fit yields $\tau \approx 32.4$ s for STP, while the memory level ($M_e$) of LTP can remain stable for at least 3 d or even longer (inset of Figure 4). Both retention times are of the same order of magnitude as those of short-term and long-term memory in the human brain. Furthermore, we study the relaxation processes of STP after different numbers of stimulation pulses were applied to the device. It is shown in **Figure 5** that, with increasing number of stimulations, the relaxation time $\tau$ increases from several seconds to tens of seconds and tends to saturate beyond 100 stimulations, indicating a decreasing forgetting rate; meanwhile, the ratio of memory retention increases slightly from around 37% to around 52%. Similar phenomena have very recently been reported by Ohno et al. and Chang et al., and are thought of as a clear indication of the STP-to-LTP transition, which is achieved through repeated stimulation.[10,13]

A more interesting phenomenon, similar to the " learning-experience" behavior of human beings,[24] was also observed. When the synaptic device is stimulated again from the mid-state, only four pulse stimulations can make the device recover its memory to the original level, as shown in Figure 4c. In contrast, dozens of pulses are required to produce the same amount of memory in the first process. After the memory recovery, the increment of memory in each stimulation returns to normal. These results indicate that the synaptic device that has " learning-experience" would allow re-learning of the forgotten information to be easier. If the STP and re-stimulation processes illustrated in Figure 4 are continued for more cycles, the preliminary results show that fewer and fewer stimulation pulses are required for memory recovery, and a behavior similar to STP-to-LTP transition occurs. Further research is in progress.

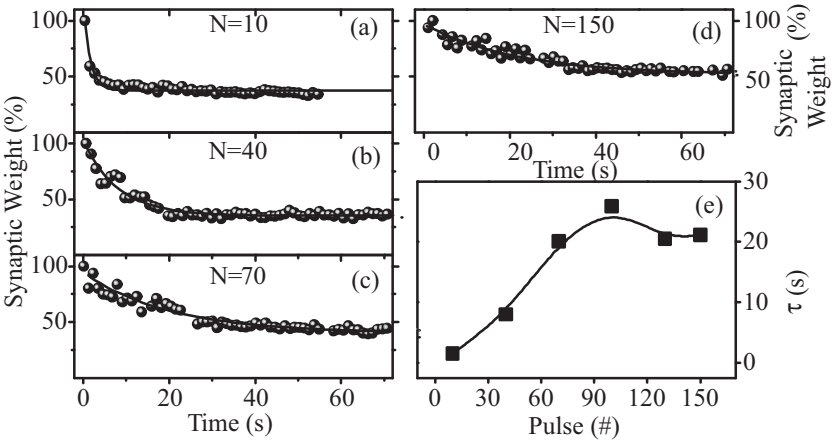


**Figure 5.** Repeated-stimulation-induced STP-to-LTP transition. a–d) Memory decay curves recorded after different numbers of identical stimuli (dots), the data have been normalized and fitted by Equation 1 (solid lines). e) The variation of relaxation time constant ($\tau$) with the number of stimulation pulses, where the $\tau$ is obtained by fitting data from a–d. The results indicate that the forgetting rate can decrease and the ratio of memory retention can increase through repeated stimulation.

Several important temporal characteristics, including spike-rate-dependent plasticity, STDP, LTP, and STP, have been demonstrated in the current synaptic device. They are not isolated but inter-related. For example, i) frequent stimulation can cause an enhancement of LTP, both spike-rate-dependent plasticity and STDP are the same on this point; and, ii) the STP-to-LTP transition can occur through repeated "stimulation" training. Obviously, the physical mechanism underlying these phenomena is different, which is discussed next.

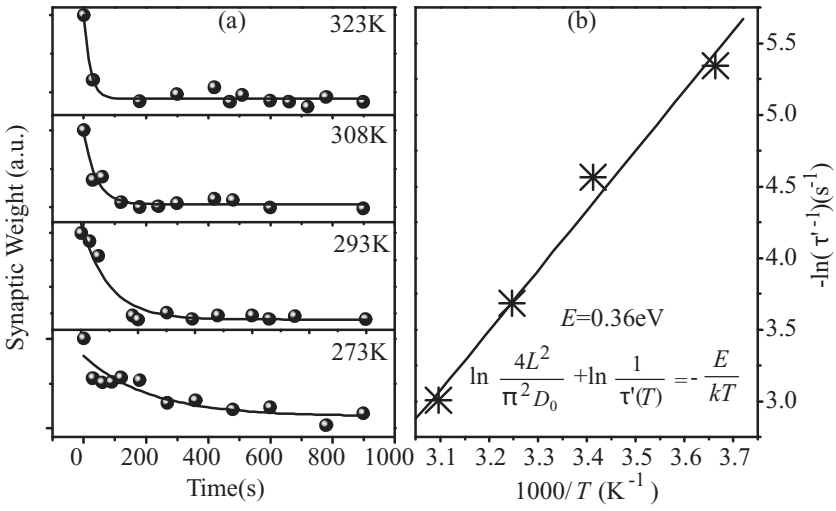


**Figure 6.** a) Memory retention data recorded at different temperature (dots) and fitted curves using Equation 1 (solid lines). b) Plot of $-\ln(\tau'^{-1})$ against $1000/T$. A linear fit using Equation 3 gives the activation energy for diffusion $E = 0.36$ eV and the room-temperature diffusion coefficient $D(T) = 2.12 \times 10^{-14}$ cm$^2$ s$^{-1}$. Both values are close to those reported for oxygen ions.[27]

## 5. Mechanism of Device Operation

Since Williams's group proposed ion migration as the basis of memristor operation,[6] several groups have built memristors based on Ag or oxygen ion migration. Such a mechanism is also applicable to the current α-IGZO memristor.[8–13] The conductance of α-IGZO depends strongly on its oxygen content: the higher oxygen content, the lower the conductivity. The movement of oxygen ions induced by electric field can change the relative thicknesses of oxygen-deficient and oxygen-rich layers, thus modulating the device conductance. However, as mentioned above, some phenomena, especially STP, cannot be understood in terms of the ion migration model. Since the oxygen ion migration can lead to differences in oxygen concentration distribution, another dynamic process, concentration-gradient-induced ion diffusion, becomes non-negligible. According to Gramm et al.,[25] assuming a linear relationship between oxygen concentration and conductivity, the solution of the one-dimensional diffusion equation can be written as:

$$\sigma(t) \approx \sigma_e + (64/\pi^2)(\sigma_0 - \sigma_e)\exp(-t/\tau'(T)) \quad (2)$$

where the $\sigma(t)$, $\sigma_0$, and $\sigma_e$ are the conductivity at time $t$, $t = 0$, and on reaching a steady state after a long time, and the $\tau'(T)$ is the relaxation time constant of the diffusion process (only the first term of the solution is given herein, the error caused by neglecting the other terms is less than 10%). Obviously, this equation has the same form as the above exponential decay equation (Equation 1) used to fit the relaxation process of STP, suggesting that the back-diffusion of oxygen ions may be responsible for STP behavior. It is known that the diffusion rate is a function of temperature ($T$). If the STP is related to oxygen ion diffusion, the relaxation process of STP will be affected by the temperature. **Figure 6** presents the decay curves of STP measured at different temperature. As expected, the relaxation time of STP is sensitive to the temperature, and increases as the temperature drops. The relaxation time of the diffusion process ($\tau'(T)$) and the diffusion coefficient $D(T)$ can be expressed as $\tau'(T) = 4L^2/\pi^2 D(T)$ and $D(T) = D_0\exp(-E/kT)$, respectively. Combining the two expressions together, we obtain

$$\ln\frac{4L^2}{\pi^2 D_0} + \ln\frac{1}{\tau'(T)} = -\frac{E}{kT} \quad (3)$$

where $E$ represents an activation energy for diffusion, $D_0$ and $L$ are the maximum diffusion coefficient at infinite temperature and the width of the initial concentration ($L \approx 20$ nm, which is roughly estimated from the active layer thickness[26]), respectively, and $k$ is the Boltzmann constant. Letting the relaxation time constant ($\tau$) of STP be equal to that of the diffusion process ($\tau'(T)$), we plotted the curve of $-\ln(\tau'^{-1})$ versus $1000/T$ using the data in Figure 6a. As shown in Figure 6b, the data approximate a straight line, as predicted in Equation 3, and the fit yields $E = 0.36$ eV. Further, the diffusion coefficient $D(T)$ at room temperature is calculated to be about $2.12 \times 10^{-14}$ cm$^2$ s$^{-1}$. Both experimental values are comparable to the activation energy (0.4 eV) and the diffusion coefficient ($5 \times 10^{-14}$ cm$^2$ s$^{-1}$) of oxygen ions reported by Nian et al.[27] This provides further evidence for the correlation between oxygen ion diffusion and STP behavior.

Considering the migration and diffusion of oxygen ions, we can understand the mechanism of device operation as follows: i) when a positive bias voltage is applied to the top electrode (oxygen-rich IGZO side), the electric field induced motion of oxygen ions compresses the highly resistive oxygen-rich IGZO layer, thus increasing the device conductivity. ii) When the bias is removed, the back-diffusion of oxygen ions (especially unstable interstitial oxygen ($O_i^{2-}$)), induced by the concentration gradient, results in a partial retreat of the conduction front, thus reducing the device conductivity. Such a dynamic process corresponds to the STP behavior. iii) When a negative pulse is applied immediately after a positive one, similar to the case of Figure 2b, the directions of ion migration and diffusion become identical, and the superposition of the two dynamic processes accelerates the retreat of the conduction front, thus resulting in the formation of a gap between the "P process" and the "N process". iv) High-rate stimulation, where the idle time between pulses is very short, can suppress the back-diffusion of oxygen ions and promote their migration and the EPSC-spike interaction. This may be a possible reason why frequent stimulation

can enhance the LTP in spike-rate-dependent plasticity and STDP behaviors. v) For amorphous materials, the structural disorder, such as bond-length and bond-angle deviations, favors the formation of unstable or metastable local structures. The back-diffusion makes a fraction of the oxygen ions recombine with oxygen vacancies ($V_o^{2+}$) or occupy interstitial lattice sites. However, these local structures are metastable, thus less energy is required to destroy their structure and make these oxygen ions migrate again, which may lead to the observation of novel "learning-experience" behavior in our device.

## 6. Conclusions

In summary, several essential synaptic functions, resembling learning/memory functions of biological systems, have been demonstrated in the α-IGZO memristor, including nonlinear transmission, spike-rate-dependent plasticity, STDP, LTP/STP, and "learning-experience" behavior. The STP decay can be well-described by a diffusion equation, and the same temperature dependence is observed between the relaxation processes of STP and ion diffusion. Both facts, along with the calculation of the diffusion coefficient, confirm that the back-diffusion of oxygen ions is a dominant mechanism of memory loss in STP. The LTP can be enhanced through two ways: high-rate stimulation with short time interval and repetitive stimulation training. The latter transfers STP to LTP. The interesting "learning-experience" characteristic is also observed, which is thought to be related to the unstable local structure in α-IGZO. Though the diffusion process and microstructural properties bring some novel features to our synaptic device, the synaptic functions and plasticity are very complex in biological systems, and more detailed consideration of some factors, such as the design of device structure, the selection of material, other dynamic mechanisms, is still needed to make the synaptic simulation more accurate and comprehensive. Studies on such physical models will also help to understand or predict, to a certain degree, some unknown mechanisms and phenomena in neuroscience.

## 7. Experimental Section

*Device Fabrication*: The memristor was composed of oxygen-deficient and oxygen-rich α-IGZO layers having the same thicknesses of approximately 40 nm. Both layers were sequentially grown on a Pt/Ti/$SiO_2$/Si substrate by magnetron sputtering at room temperature. Ultrapure argon with 1 Pa pressure and oxygen with 2 Pa pressure were used as the sputtering gases for oxygen-deficient and -rich layers, respectively. The Pt electrodes were thermally evaporated on the top and patterned into many circular pads with a diameter of 0.5 mm using a shadow mask.

*Device Test:* The device measurements were carried out using a semiconductor parameter analyzer (B1500A, Agilent), an arbitrary function generator (3390, Keithley), an oscilloscope (TDS 2012B, Tektronix), and a SourceMeter (2636A, Keithley). Both writing and reading of the memristor were performed in the pulse mode. According to Figure 1a, an electrical pulse with low amplitude (3 V) and short duration (20 or 50 ms) was used as the read voltage to minimize disturbance on device conductance. We define a flow of current from top to bottom electrode as the positive bias. In Figure 2a, three kinds of pulses with different amplitude and duration of (5 V, 50 ms), (5 V, 100 ms) and (6 V, 100 ms) were used to stimulate the synaptic device to investigate its response to stimulus intensity and duration. In Figure 2b, 100 positive pulses (amplitude 5 V, duration 100 ms) followed by 80 negative pulses (amplitude –5 V, duration 100 ms) were applied. In the above two tests, the stimulation pulse interval was extended to 1 s to suppress the spike-rate effect, and the current was read after each stimulation pulse is applied. In the studies on spike rate dependent plasticity (Figure 3a), the amplitude and duration of stimulation pulses were fixed at 5 V and 10 ms, but their interval was varied between 10, 40, 70, and 90 ms. The current is read once every 10 stimuli. The parameters of stimulation and read pulses in Figures 4a and c were identical to those of the positive pulses in Figure 2b. The decay processes of STP, shown in Figure 4b, 5 and 6, were recorded by monitoring the current change with time. To obtain the decay curves in Figure 5, we continuously stimulated the device using different numbers of pulses (amplitude 5 V, duration 20 ms, interval 30 ms), and then read the current every second with 3 V, 20 ms read pulses immediately after the last stimulus in the series. Figure 6 presents the temperature dependence of STP, where the device was stimulated by 100 consecutive pulses (amplitude 6 V, duration 100 ms, interval 100 ms) at different temperatures.

## Acknowledgements

This work was supported by the National Basic Research Program of China (973 Program) (Grant No. 2012CB933703), the National Natural Science Foundation of China (Grant Nos. 51172041 and 60907016), the Program for New Century Excellent Talents in University (Grant No. NCET-11-0615), the Fund from Jilin Province (Grant Nos. 20121802, 20100339, and 20110105), and the Fundamental Research Funds for the Central Universities (Grant Nos.10SSXT127, 10JCXK002 and 10QNJJ005).

Received: December 27, 2011
Published online: April 10, 2012

[1] G. Q. Bi, M. M. Poo, *J. Neurosci.* **1998**, *18*, 10464.
[2] G. Q. Bi M. M. Poo, *Nature* **1999**, *401*, 792.
[3] C. Diorio, P. Hasler, A. Minch, C. A. Mead, *IEEE Trans. Electron Devices* **1996**, *43*, 1972.
[4] P. Hafliger, M. Mahowald, *Analog Integr. Circuits Signal Process.* **1999**, *18*, 133.
[5] A. Bofill-i-Petit, A. F. Murray, *IEEE Trans. Neural Networks* **2004**, **15**, 1296.
[6] D. B. Strukov, G. S. Snider, D. R. Stewart, R. S. Williams, *Nature* **2008**, *453*, 80.
[7] G. S. Snider, *IEEE/ACM International Symposium on Nanoscale Architectures*, Anaheim, CA June **2008**, p. 85.
[8] K. Seo, I. Kim, S. Jung, M. Jo, S. Park, J. Park, J. Shin, K. P. Biju, J. Kong, K. Lee, B. Lee, H. Hwang, *Nanotechnology* **2011**, *22*, 254023.
[9] T. Hasegawa, T. Ohno, K. Terabe, T. Tsuruoka, T. Nakayama, J. K. Gimzewski, M. Aono, *Adv. Mater.* **2010**, *22*, 1831.
[10] T. Ohno, T. Hasegawa, T. Tsuruoka, K. Terabe, J. K. Gimzewski, M. Aono, *Nat. Mater.* **2011**, *10*, 591.
[11] Q. Lai, L. Zhang, Z. Li, W. F. Stickle, R. S. Williams, Y. Chen, *Adv. Mater.* **2010**, *22*, 2448.
[12] S. H. Jo, T. Chang, I. Ebong, B. B. Bhadviya, P. Mazumder, W. Lu, *Nano Lett.* **2010**, *10*, 1297.
[13] T. Chang, S. H. Jo, W. Lu, *ACS Nano* **2011**, *5*, 7669.
[14] Z. Q. Wang, H. Y. Xu, X. H. Li, X. T. Zhang, Y. X. Liu, Y. C. Liu, *IEEE Electron Device Lett.* **2011**, *32*, 1442.
[15] K. Nomura, H. Ohta, A. Takagi, T. Kamiya, M. Hirano1, H. Hosono, *Nature* **2004**, *432*, 488.
[16] C. C. Bell, V. Z. Han, Y. Sugawara, K. Grant, *Nature* **1997**, *387*, 278.

[17] A. R. Moreno, O. Paulsen, *Nat. Neurosci.* **2008**, *11*, 744.
[18] L. F. Abbott, S. B. Nelson, *Nat. Neurosci.* **2000**, *3*, 1178.
[19] L. I. Zhang, H. W. Tao, C. E. Holt, W. A. Harris, M. M. Poo, *Nature* **1998**, *395*, 37.
[20] M. Mori, M. H. Abegg, B. H. Gahwiler, U. Gerber, *Nature* **2004**, *431*, 453.
[21] T. V. P. Bliss, G. L. Collingridge, *Nature* **1993**, *361*, 31.
[22] G. Daoudal, D. Debanne, *Learn. Mem.* **2003**, *10*, 456.
[23] C. F. Stevens, J. F. Wesseling, *Neuron* **1999**, *22*, 139.
[24] W. T. Greenough, J. E. Black, C. S. Wallace, *Child Dev.* **1987**, *58*, 539.
[25] A. Gramm, Th. Zahner, U. Spreitzer, R. Rossler, J. D. Pedarnig, D. Bauerle, H. Lengfellner, *Europhys. Lett.* **2000**, *49*, 501.
[26] D. Kwon, K. M. Kim, J. H. Jang, J. M. Jeon, M. H. Lee, G. H. Kim, X. Li, G. Park, B. Lee, S. Han, M. Kim, C. S. Hwang, *Nat. Nanotechnol.* **2010**, *5*, 148.
[27] Y. B. Nian, J. Strozier, N. J. Wu, X. Chen, A. Ignatiev, *Phys. Rev. Lett.* **2007**, *98*, 146403.